Assessing the sensitivity of multi-frequency passive microwave vegetation optical depth to vegetation properties

Luisa Schmidt[1], Matthias Forkel[1], Ruxandra-Maria Zotta[2], Samuel Scherrer[2], Wouter A. Dorigo[2], Alexander Kuhn-Régnier[3,4], Robin van der Schalie[5], Marta Yebra[6,7]

[1] Technische Universität Dresden, Institute of Photogrammetry and Remote Sensing, 01069 Dresden, Germany
[2] Technische Universität Wien, Department of Geodesy and Geoinformation, Vienna, Austria
[3] Leverhulme Centre for Wildfires, Environment, and Society, London, SW7 2AZ, UK
[4] Department of Physics, Imperial College London, London, SW7 2AZ, UK
[5] Planet, Wilhelminastraat 43A, 2011 VK Haarlem, The Netherlands
[6] Fenner School of Environment & Society, Australian National University, ACT 2601, Australia
[7] School of Engineering, Australian National University, ACT 2601, Australia

Correspondence to: Luisa Schmidt (luisa.schmidt1@tu-dresden.de)

Abstract. Vegetation attenuates the microwave emission from the land surface. The strength of this attenuation is quantified in models in terms of the parameter Vegetation Optical Depth (VOD), and is influenced by the vegetation mass, structure, water content, and observation wavelength. Earth observation satellites operating in the microwave frequencies are used for global VOD retrievals, enabling the monitoring of vegetation status at large scales. VOD has been used to determine above-ground biomass, monitor phenology or estimate vegetation water status. VOD can be also used for constraining land surface models or modelling wildfires at large scale. Several VOD products exist differing by frequency/wavelength, sensor, and retrieval algorithm. Numerous studies present correlations or empirical functions between different VOD datasets and vegetation variables such as normalised difference vegetation index, leaf area index, gross primary production, biomass, vegetation height or vegetation water content. However, an assessment of the joint impact of land cover, vegetation biomass, leaf area, and moisture status on the VOD signal is challenging and has not yet been done.

This study aims to interpret the VOD signal as a multi-variate function of several descriptive vegetation variables. The results will help to select certain VOD wavelengths for specific applications and can guide the development of appropriate observation operators to integrate VOD with large-scale land surface models. Here we use VOD from the Land Parameter Retrieval Model (LPRM) of Ku-, X- and C-bands of the harmonised VODCA dataset and level 3 L-band derived from SMOS and SMAP sensors. Within a multivariable regression random forest model for simulating these VOD signals, leaf area index, live-fuel moisture content, above-ground biomass, and land cover are able to explain up to 0.95 of the variance (coefficient of determination). Thereby, the variance in L-band VOD is reproduced spatially and for Ku-, X- and C-band VOD spatially as well as temporally. Analyses of accumulated local effects demonstrate that Ku-, X- and C-band VOD is mostly sensitive to leaf area index and L-band VOD to above-ground biomass. However, for all VODs the global relationships with vegetation properties are non-monotonic and complex and differ with land cover type. This indicates that the use of simple global regressions to estimate single vegetation properties (e.g. above-ground biomass) from VOD is over-simplistic.

1 Introduction

Vegetation Optical Depth (VOD) describes the attenuation by the vegetation layer of microwave radiation emitted by the Earth. Quantifying this effect is important for an accurate retrieval of surface soil moisture from passive microwave satellite observations (Wang, 1985; Njoku and Entekhabi, 1996). In the radiative transfer equation for microwave emissions, the opacity of the vegetation layer (i.e. the VOD) is also commonly referred to as τ (Jackson et al., 1982). VOD can be retrieved e.g. from the passive microwave radiative transfer equation using measurements of passive microwaves (Jackson and Schmugge, 1991;

Owe et al., 2008; Sawada et al., 2016). However, it is not directly measurable and verifiable with in-situ measurements, which is why different authors have correlated VOD with different vegetation properties to understand what VOD is sensitive to. Generally, the opacity of passive microwaves in the vegetation layer increases with increasing vegetation water content but

45   this relationship varies with vegetation structure including leaf and woody components and wavelength (Jackson and Schmugge, 1991; Wigneron et al., 1993; Njoku and Entekhabi, 1996). Based on radiometer measurements over various crops and a wide range of wavelengths (0.8 – 30 cm), Jackson and Schmugge (1991) report a clear linear relationship of VOD to vegetation water content (VWC):

VOD = b * VWC,   (1)

50   where the parameter b depends on vegetation type and wavelength. The authors find that b exponentially decreases with increasing wavelength, which implies that vegetation opacity (the VOD) is smaller for longer wavelengths (i.e. L-band) than for shorter wavelengths (i.e. Ku-, X- and C-bands). The vegetation water content can also be expressed as a product of above-ground biomass (AGB) and a relative water content parameter, often referred to as live-fuel moisture content (LFMC) (Konings et al., 2019):

55   VOD = b * AGB * LFMC.   (2)

Based on those relationships, many studies use VOD to estimate AGB or other vegetation properties. For example, Liu et al. (2015) use Ku-band VOD to estimate long-term changes in global AGB, finding a gain of above-ground biomass carbon considering forest and non-forest vegetation for 1993-2012. Rodríguez-Fernández et al. (2018) correlate spatial patterns in AGB and yearly averaged values of L-band VOD from the Soil Moisture and Ocean Salinity mission with the INRA-CESBIO

60   algorithm (SMOS-IC) for Africa with correlation coefficients up to 0.85. They find linear relationships between VOD and AGB within single land cover classes, but the relationship across land cover classes is shown to be nonlinear, with a weaker nonlinearity for L-band VOD compared to Ku-/X-/C-band VOD. Chaparro et al. (2018) use L-band from the Soil Moisture Active Passive mission (SMOS) derived with the Multi-Temporal Dual Channel Algorithm (MT-DCA) to determine crop biomass of the north-center of the USA. Both Rodríguez-Fernández et al. (2018) and Chaparro et al. (2018) find better results

65   for pixels with higher homogeneity, not just for land cover types but even for plant types, implying that relationships between VOD and vegetation properties change with land cover and plant types. Li et al. (2021b) find high correlation of L-band VOD and AGB leading to the conclusion that longwave VOD is more sensitive to woody parts of the vegetation than shortwave VOD. However, Konings et al. (2021) show that the relation between L-band VOD and AGB dominates in space but that short-term temporal dynamics in VOD are dominated by VWC. As a proxy for vegetation water status, VOD can be related to

70   LFMC or VWC or both (Fan et al., 2018; Konings et al., 2019; Frappart et al., 2020) and can be used to estimate leaf water potential (Konings and Gentine, 2017; Momen et al., 2017; Zhang et al., 2019).

Furthermore, VOD is frequently compared with other vegetation properties such as canopy greenness, leaf area index (LAI), or plant productivity. For example, VOD shows similar temporal patterns to normalised difference vegetation index (NDVI) and LAI (Liu et al., 2011; Momen et al., 2017; Bousquet et al., 2021). In spatial comparisons, the vegetation indices and

75   variables tend to saturate over densely vegetated areas. This saturation is less distinct for VOD (Rodríguez-Fernández et al., 2018) due to the ability of microwaves to penetrate deeper into the vegetation layer. VOD can therefore provide complementary information to the usually visible-infrared based metrics, e.g. for assessments of land surface phenology (Jones et al., 2011). Metrics sensitive to biomass or water content shifts can be derived from VOD (Jones et al., 2011, 2014). VOD and temporal changes in VOD are also correlated with gross primary production (GPP) (Teubner et al., 2018), which allowed to develop a

80   sink-driven GPP estimation approach based on VOD (Teubner et al., 2019, 2021; Wild et al., 2022).

Recently, several new VOD datasets became available for X-band from the Advanced Microwave Scanning Radiometer – Earth Observing System sensor (AMSR-E) and Advanced Microwave Scanning Radiometer 2 (AMSR2) sensors (Du et al., 2017; Wang et al., 2021), in L-band from SMOS (van der Schalie et al., 2016; Fernandez-Moran et al., 2017; Al Bitar et al., 2017; Wigneron et al., 2018, 2021) and SMAP (Konings et al., 2017), or Ku-, X- and C-band from several sensors (van der

85   Schalie et al., 2017) as well as harmonized datasets (Vegetation Optical Depth Climate Archive VODCA, Moesinger et al., 2020). A recent comparison study by Li et al. (2021) of different X-, C- and L-band VOD datasets and Moderate Resolution Imaging Spectroradiometer (MODIS) derived vegetation indices like NDVI and enhanced vegetation index (EVI) as well as tree height and AGB showed that X-band VOD is more suitable to detect temporal variations of the green vegetation parts, especially for less densely vegetated areas, than C- and L-band VOD. Additionally, Li et al. (2021) as well as Moesinger et al.

90   (2022) found time lags between VOD and vegetation indices and climate variables, showing the need to include a further vegetation property to improve the response of VOD to temporal changes in the vegetation status. To take into account VOD variations caused by vegetation water content more complex than simple regression functions have been developed (e.g. Momen et al., 2017). Momen et al. (2017) were able to estimate VOD by using two predictors, LAI and leaf water potential. Teubner et al. (2019) linked VOD and GPP by using generalized additive models and the differential equation between VOD

95   and AGB by Liu et al. (2015). Among others, these two studies show that the water content of the vegetation is not only influencing the relation between vegetation indices and VOD but also the relation between VOD and AGB.

The increasing availability of VOD data for vegetation studies also increases the possibilities to assimilate or integrate VOD with ecosystem or land surface models (LSM) (Scholze et al., 2019; Kumar et al., 2020). Therefore, observation operators are needed that link the modelled vegetation properties with the satellite-retrieved VOD. Scholze et al. (2019) use a sum of an

100   empirical AGB function and a linear term for LAI to describe annual SMOS-IC L-band VOD within the Carbon Cycle Data Assimilation System (CCDAS) for estimating European carbon fluxes. Kumar et al. (2020) use CDF matching to convert VODCA X- and C-band VOD, and SMAP L-band VOD to LAI, which is then assimilated into the Noah-MP LSM. X- and L-band VOD showed partially complementary improvements of the modelled land surface variables. Both studies by Scholze et al. (2019) and Kumar et al. (2020) find an improvement of the model results by incorporating passive microwave data,

105   demonstrating the benefits of the vegetation information contained in VOD. In another model-data-fusion approach, Liu et al., 2021 use VOD to derive plant hydraulic parameters for a soil-plant system model that accounts for the hydraulic state of the vegetation explicitly. However, as VOD reflects both dynamics in biomass and water content (Jackson and Schmugge, 1991; Konings et al., 2021), relations between VOD and AGB or LAI as observation operators are simplifications and demonstrate the need for a more detailed understanding of the effects of vegetation properties on VOD.

110

The increasing use of VOD for ecosystem studies (e.g. Dorigo, 2021) and land surface modelling poses the question how different vegetation properties affect VOD in both time and space. Hence, a more detailed investigation of the relative effects of vegetation properties on VOD could improve the understanding of the VOD signal in terms of interpretation of the corresponding vegetation status. Such investigations will also help to identify a suitable VOD dataset for a specific ecological

115   application. Furthermore, due to the high temporal resolution and temporal coverage of VOD datasets (partly since 1987), global analyses of vegetation properties and status as well as land cover change can be conducted for enhanced understanding of long-term environmental changes and to improve model predictions.

Here we aim to assess VOD in response to multiple vegetation properties at large (i.e. inter-continental) scales. We apply a multi-variate framework using machine learning approaches (random forest, RF and generalized additive model, GAM) to

120   quantify sensitivities of VOD to and interactions with LFMC, LAI, AGB, and land cover. Generalized additive models and random forests are used to predict VOD from vegetation properties and accumulated local effect (ALE) curves are used to assess the sensitivities of VOD to these properties. Comparing both machine learning algorithms gives insights into the structure of the relationship between VOD and vegetation properties and provides confidence in the findings. Additionally, we inspect how different temporal resolutions (i.e. 8-daily and monthly data) affect the relationships between VOD and vegetation

125   properties for identifying the role of vegetation variables at quasi-weekly and seasonal time scales. The analyses are carried out for five VOD datasets, which differ in wavelength but were derived with the same algorithm (Land Parameter Retrieval Model, LPRM) (van der Schalie et al., 2016; van der Schalie et al., 2017) to exclude differences due to retrieval algorithms.

2 Data and methods

2.1 Datasets

130 #### 2.1.1 VOD data

An overview of the datasets is given in Table 1 and Figure 1. All used VOD datasets are derived from passive sensors using the LPRM algorithm (van der Schalie et al., 2016).

The VODCA dataset (Moesinger et al., 2020) provides harmonised long-term records of shortwave VOD for Ku-, X- and C-band (further named Ku-VOD, X-VOD and C-VOD, respectively), using data from the AMSR-E, AMSR-2, Special Sensor

135 Microwave Imager (SSM/I), TRMM Microwave Imager (TMI), and Windsat sensors. Unfortunately, Ku-VOD is only available until 1st August 2017 due to a bias in the eleven brightness temperatures of AMSR-2 causing unexpected low values of the VOD retrievals after this date (Moesinger et al., 2020), which is not fixed in the version 01.0. Therefore, all datasets are analysed until 31st July 2017.

Two LPRM-derived L-band VOD datasets are used as longwave VOD, one sensed with SMAP, the other with SMOS (Schalie

140 et al., 2016, further named as SMAP L-VOD and SMOS L-VOD, respectively). The SMAP satellite was launched in January 2015, and therefore SMAP L-VOD defines the start date of the analysis of all datasets.

All VOD datasets are provided as daily data with a spatial resolution of 0.25° on a global scale. As VOD generally decreases with increasing wavelength, the five VOD datasets have different dynamic ranges. As we are not interested in the absolute value but only the temporal dynamics and spatial patterns, the VOD datasets were globally normalised using minimum and

145 maximum value to a range of 0 to 1 based on the available global data within the time span 2015-2017 to provide comparability. For normalising we use the scikit-learn function 'MinMaxScaler'.

2.1.2 Predictor data

Following the relationship between VOD, LFMC, and AGB as shown in equation 2, proxies related to biomass (AGB and LAI), water content (LFMC), and the structure parameter (plant types) are used as predictors for VOD.

150 As proxies for woody and non-woody biomass, we used a map of AGB and a time series of LAI. The ESA CCI AGB map (Santoro and Cartus, 2019) for the year 2017 with 100 m spatial resolution is used as a predictor for woody biomass. This AGB map describes the oven-dry mass of woody parts of living trees per pixel. Thereby only above-ground mass is considered, i.e. stem and bark as well twigs and branches, but not stumps and roots.

LAI is used as a proxy for canopy biomass. Specifically, we use the MOD15A2H version 6 dataset from MODIS, which is

155 available at 500 m spatial and on a 8-daily temporal resolution on a global scale (Myneni et al., 2015). We excluded LAI retrievals under (partial) cloud cover, snow or high solar zenith angle.

For live fuel moisture content, we used a product derived from MODIS Collection 6 for three regions (California/western US, South Africa and Australia) at a 500 m spatial and on a 4-daily temporal resolution using the approach described in Yebra et al. (2018). Additionally, we used a European product computed by the European Union Joint Research Centre (JRC) for the

160 European Forest Fire Information System (EFFIS). This product uses also methods described in Yebra et al. (2018) but MODIS Collection 5. Therefore, it is produced with a temporal resolution of 8 days.

The LAI, LFMC, as well as the AGB datasets were resampled to 0.25° resolution to match the VOD spatial extent using a first order conservative remapping.

We used the land cover map by the European Space Agency (ESA) Climate Change Initiative (CCI, ESA, 2017) and its

165 continuation from the Copernicus Climate Change Service which provide yearly data for the period 1992-2018 at 300 m spatial resolution. The land cover classes were converted to fractions of plant functional types and aggregated to 0.25° spatial resolution using the cross-walking approach as described in Poulter et al. (2015). Specifically, we made use of the fractions per 0.25° grid cell of broad-leaved evergreen (treeBE), needle-leaved evergreen (treeNE), deciduous trees (treeD), shrublands

(shrub), croplands (crop), and herbaceous vegetation (herb). Deciduous trees were not further segregated into broad- and

170 needle-leaved trees as especially the latter would result in only a small sample when intersected with the VOD data. In another test, we also combined the fractional coverage of all tree PFTs (treeAll = treeBE + treeNE + treeD) and of short vegetation (short = shrub + herb + crop).

Table 1: Overview of datasets used and technical attributes.

Dataset	Variable and unit	Sensors	Temporal coverage / resolution	Spatial coverage / resolution	Reference
VODCA v01.0	Ku-VOD (-)	AMSR-2, SSMI/I, TMI and Windsat scaled to AMSR-E	1987-2017 / daily	Global / 0.25°	Moesinger et al. (2020)
	X-VOD (-)*		1997-2018 / daily		
	C-VOD (-)**		2002-2018 / daily		
SMAP L-VOD	L-VOD (-)	SMAP radiometer	2015-2019 / daily		van der Schalie et al. (2016)
SMOS L-VOD	L-VOD (-)	MIRAS	2010-2020 / daily		
ESA CCI AGB v1.0	AGB (Mg/ha)	PALSAR-2, Sentinel-1 (1A and 1B), Landsat	2017 / representative for one year	Global / 100 x 100 m	Santoro and Cartus (2019)
MOD15A2H v006	LAI (-)	MODIS sensors	2000-2020 / 8-daily	Global / 500 x 500 m	Myneni et al.(2015)
MODIS-LFMC	LFMC (%)	MODIS sensors	2000-2019 / 4-daily	Regional / 500 x 500 m California, South Africa, Australia	Yebra et al. (2018)
			8-daily	Europe	
ESA CCI Land cover v2.0.7	Plant functional types (PFT) derived from land cover classes	AVHRR, PROBA-V, Envisat MERIS, SPOT-VGT	1992-2018 / yearly	Global / 300 x 300 m	ESA (2017)

175 * does not contain SSM/I ** does not contain SSM/I and TMI
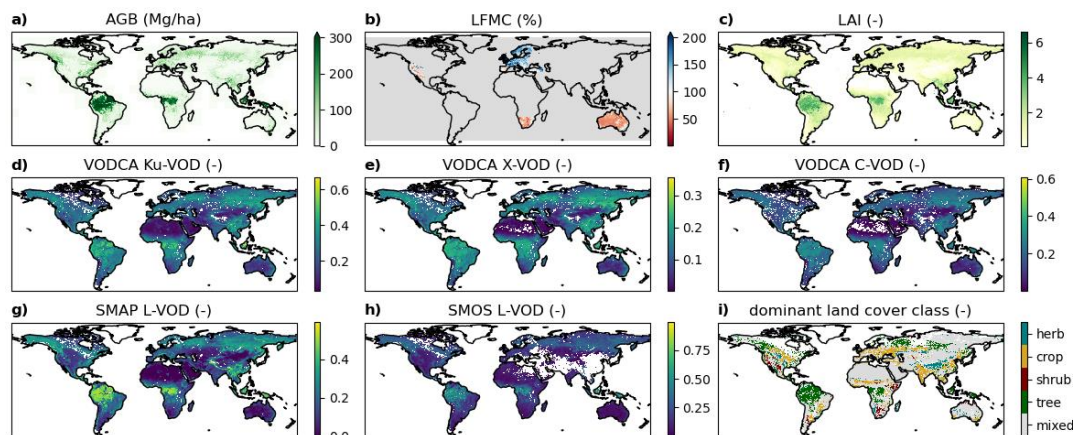
Figure 1: Overview of the datasets used a) Above-ground biomass (AGB) for 2017 based on the ESA CCI biomass dataset, b) Live Fuel Moisture Content (LFMC) derived from MODIS whereby grey indicates areas of non-available data, c) Leaf Area Index (LAI) derived from MODIS, d) Ku-band VOD (Ku-VOD) from VODCA, e) X-band VOD (X-VOD) from VODCA, f) C-band VOD (C-

180 **VOD) from VODCA, g) L-band VOD from SMAP (SMAP L-VOD), h) L-band VOD from SMOS (SMOS L-VOD), and i) the dominant land cover class for 2016 based on the ESA CCI land cover map. LAI, LFMC, and VOD maps are temporal averages over the period January 2015-July 2017. Note LFMC is only available for California, Southern Africa, Europe, and Australia.**

2.1.3 Data combination

All datasets were cropped to the extent of the LFMC data (Australia, Europe, California, South Africa) for further analyses.
185 This implies that the 'global' models as stated in the following are indeed inter-continental models restricted to the spatial extent of the LFMC dataset. To provide comparability of the analyses of the different VOD datasets, only the overlapping timespan is used (January 2015-July 2017). The rather short time period does not impede the framework of this study, because instead of analysing coherent pixel time series this approach uses each time step of each pixel as an individual data point. The ESA CCI AGB map represents the year 2017, but we assume that the biomass does not dramatically change over two years.
190 Therefore, the AGB values are kept constant for the whole time series. The PFT fractions are taken from the annual land cover maps for the respective years in 2015 to 2017 without any interpolation. During the analyses, models were trained and tested for 8-daily and monthly temporal resolutions of the LAI and LFMC time series. For the 8-daily resolution, only the VOD values matching the same timestamp of the MODIS LAI and LFMC products are used. For the monthly resolution, the mean VOD, LAI or LFMC within the regarding month were calculated.

195 As a final step, pixels were excluded when the fractional coverage of bare ground or water exceeds 5 % to avoid the interpretation of marginal effects of bare soils or water on VOD. Models were specifically trained for single land cover classes. A threshold of 55 % was used to discern when a land cover class was dominant compared to the other classes.

2.2 Regression methods

To assess the influence of the vegetation variables on VOD, we applied two methods: generalized additive models (GAM) and
200 random forest regressor (RF). Both methods are compared to evaluate if the relationship between the features and the predictor variable is rather simple additive assembled (adequately captured by GAM) or more complex (requires RF). GAM can represent non-linear and non-monotonic relations with single predictors whereby all predictors have a joined additive effect. RF can represent more complex relations and interactions between the single predictors, but are not well suited for capturing additive structures in the data (Hastie et al., 2009). Another reason to use GAM simultaneously to RF is that models that are
205 designed for short vegetation use just two predictors (LAI and LFMC). AGB is only representative for woody biomass of trees and can therefore not be included for short vegetation. While GAMs can utilise a small number of predictors, the application of RF with only two predictors will likely result in overfitting as the random choice of a predictor variable during the development of decision trees is very limited. Both methods allow the qualitative and quantitative assessment of the sensitivities of VOD to the predictors via Accumulated Local Effects (ALE, see chapter 2.5).
210 The RF algorithm incorporates multiple independent decision trees, where the final prediction is the average prediction of the individual trees (Breiman, 2001; Hutengs and Vohland, 2016; Liang et al., 2018). Using the scikit-learn package (version 24.1), multiple hyper-parameters can be tuned. During a grid-search using the scikit-learn function 'RandomizedSearchCV' for an exemplary dataset (predicting monthly inter-continental Ku-VOD with LAI, LFMC, AGB, and land cover), the minimum number of samples within a leaf (1 and 4), number of estimators (100, 200-2000 with 200-steps), maximum features
215 (functions: 'auto', 'sqrt', 'log2'), maximal depth (10-110 with 20-steps, None), and minimum samples split (2 and 10) were tested. The best combinations were again tested with monthly inter-continental predictions of X-, C-, SMOS and SMAP L-VOD. Some combinations led to partly improved results compared to the scikit-learn default hyper-parameters, but also partly degraded results. We finally selected the following hyper-parameters: minimum samples within a leaf=1, number of estimators=100, maximum features='auto', maximal depth=None, minimum samples split=2 and criterion=mean squared
220 error. This setup provided across all tested models the best results. The chosen maximum features parameter leads to the consideration of all features for all splits, thereby omitting one of the strengths of RF. This parameter may have been selected

due to the low number of our chosen vegetation variables. RF is still able to capture complex relationships, which is our main focus.

GAMs are a progression of standard linear regression models and generalized linear models (GLMs) (Hastie and Tibshirani,
225 1987). In comparison to standard linear regression models, GLMs use a link function to connect the mean response of the target variable with the predictors, which can also represent other distributions of the target variable besides the Gaussian distribution, like binomial, gamma or Poisson distributions (Nelder and Wedderburn, 1972). In addition, GAMs incorporate smoothing functions for each predictor variable (Yee and Mitchell, 1991). This allows modeling non-linear and non-parametric relationships between the target and predictor variables. A general GAM equation can be written as:

230 $$g(\mu) = b + \sum_{i=1}^{p} f_j(x_i)\,,$$ (3)

with g() as link function, μ as mean response of target variable, b as intercept term, f() as smoothing functions, and x as predictor variables. Here the GAM is developed for a Gaussian distribution with an 'identity' link function and spline terms as smoothing functions using the Python package pyGAM (version 0.8.0).

2.3 Model experiments

235 We applied two main classes of regression models to predict VOD. The first class are global models that use the PFTs from the land cover map in addition to the vegetation predictors LAI, LFMC, and AGB. This means that the individual maps of treeBE, treeBD, treeNE, treeND, shrub, crop, and herb are used as additional predictors. The second model class is comprised of land cover–specific models using LAI, LFMC, and AGB as inputs. These models are only applied to the spatial extent of one dominant land cover class. In models for short vegetation classes, AGB is not used as a predictor because this map is only
240 representative of forest biomass. All model setups were trained both for GAM and RF, and using monthly as well as 8-daily values for each VOD dataset. Table 2 gives an overview of the models and the input data.

Table 2: List of tested models, with N = needleleaf, B = broadleaf, E = evergreen, D = deciduous, All = not differentiated, CCI PFT = ESA Climate Change Initiative Plant Functional Type; each model is run with GAM and RF as well as with datasets with 8-daily
245 **and monthly temporal resolution for each VOD dataset.**

Land cover class/ Model name	Spatial domain (defined by dominant land cover)	Predictors
Land cover-specific models		
treeAll	CCI PFT treeAll > 55%	AGB + LFMC + LAI
treeNE	CCI PFT treeNE> 55%	AGB + LFMC + LAI
treeBE	CCI PFT treeBE > 55%	AGB + LFMC + LAI
treeB	CCI PFT (treeBE + treeBD) > 55%	AGB + LFMC + LAI
treeN	CCI PFT (treeNE + treeND) > 55%	AGB + LFMC + LAI
treeD	CCI PFT (treeBD + treeND) > 55%	AGB + LFMC + LAI
treeE	CCI PFT (treeBE + treeBD) > 55%	AGB + LFMC + LAI
shrub	CCI PFT shrub > 55%	LFMC + LAI
crop	CCI PFT crop > 55%	LFMC + LAI
herb	CCI PFT herb > 55%	LFMC + LAI
short vegetation	CCI PFT (shrub + crop + herb) > 55%	LFMC + LAI
Global model (including land cover as predictor)		
global	inter-continental (all grid cells in southern Africa, California, Australia, and Europe)	AGB + LFMC + LAI + treeNE + treeND + treeBE + treeBD + shrub + crop + herb

2.4 Model evaluation

For the evaluation of the models, 5-fold cross-validation is used. The same randomly computed folds are used for RF and GAM. The results are averages across all folds. The performance of the models is evaluated using the coefficient of
250 determination (R^2) and root mean squared error (RMSE) between the satellite-derived and the modelled VOD. R^2 commonly

ranges between 1 (perfect agreement) and 0, where the latter is the score for a model which solely predicts the mean of the reference data. Models that perform worse than this can also yield negative R^2 values. In addition to the overall evaluation of the models, we evaluate the spatial distribution of R^2, i.e. R^2 of the satellite and modelled VOD time series.

2.5 Partial relationships: Accumulated Local Effects (ALE)

255   The relationships and sensitivities of VOD to the predictors are examined via Accumulated Local Effects (ALE) plots (Apley and Zhu, 2020). ALE plots are improvements over Partial Dependence Plots (PDP) (Friedman, 2001; Kuhn-Régnier et al., 2021) but can be interpreted similarly, i.e. as a partial relationship between a predictor and the target variable, taking into account all other predictors. Unlike PDPs, ALE does not combine each plotted predictor value with all possible combinations of the other predictors. For ALE, evenly spaced quantiles across the range of an examined feature are defined. Every such

260   quantile is then combined with the closest, existing value combinations of all other features. This procedure prevents unlikely and unrealistic feature combinations, which increases robustness, especially when features are strongly correlated. The ALE plots were generated from the final models, where all available data were used for training.

To quantify the influence of the predictors on the target variable, we calculated the amplitude of the ALE curve (Δ_A).

3 Results

265   **3.1 Performance of the models**

The different regression models used to predict satellite-derived VODs showed large differences in model performance (-0.04 ≤ R^2 ≤ 0.97; 0.004 ≤ RMSE ≤ 0.2) (Figure 2, Figure S1 and S2 in supplement). This difference was dominated by 1) the type of regression model (RF or GAM), 2) by the use of 8-daily or monthly data, 3) by the inclusion of land cover information as a predictor (land cover-specific vs. global models, 4) the wavelength of the predicted VOD (i.e. from Ku- to L-band), and 5) by

270   the vegetation type which the model is applied to, i.e. spatial variability of global model performance, which will be discussed in more detail in the following.
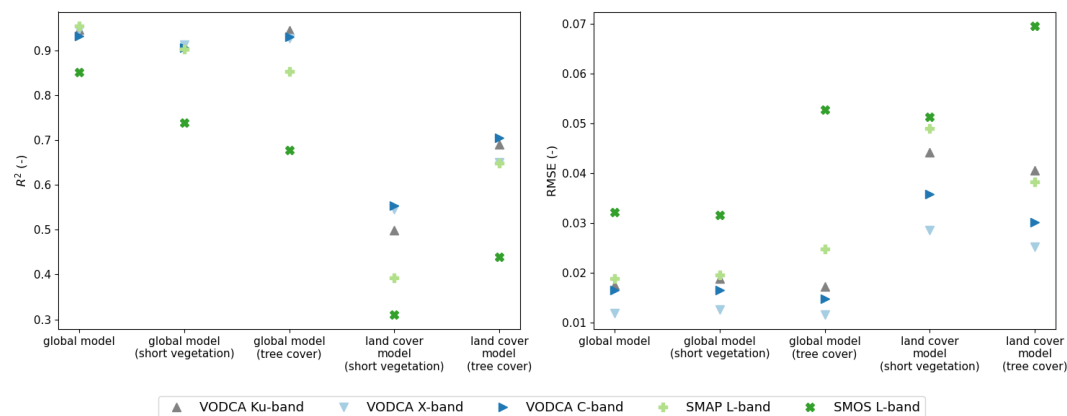
Figure 2: Coefficient of determination (R^2, left) and RMSE (right) of random forest (RF) models using monthly data. The global model uses PFTs as predictors, contrary to the land cover models, which were calibrated and applied only to the spatial extent of a
275   **certain dominant land cover class. Global model short vegetation and tree cover uses results of the global model, but filtered by dominant land cover class.**

3.1.1 Effect of the type of regression model used for calibrating the models (RF vs. GAM)

In general, RF performed better than GAM in predicting VOD, except for land cover-specific models for short vegetation classes where GAM reached similar or slightly higher performance than RF (Figure S1, Figure S2 for corresponding RMSE

280 results). In most cases, GAMs underestimated high VOD values. Based on these findings, in the following sections, we only refer to the results of RF models. If not stated otherwise, similar results were found for GAM.

3.1.2 Effect of the temporal aggregation of the explanatory variables (8-daily vs. monthly data)

Regression models based on monthly data had higher R^2 and lower RMSE than models based on 8-daily data (Figure S1 and S2). The superior performance of monthly over 8-daily models increased with increasing wavelength. For example, the

285 difference was especially large for the prediction of SMOS L-VOD for which R^2 doubled from 8-daily to monthly data (Figure S1). The performance in predicting Ku-, X- or C-VOD was similar or monthly data presented slightly higher performance than 8-daily data. Given the higher performance of models based on monthly data, the following description of results is based on these, unless mentioned otherwise.

3.1.3 Effect of including land cover information as a predictor (global vs. land cover-specific models)

290 Considering RF models based on monthly data, the global models (defined as models including fractional cover of PFTs as predictors, see Table 2) showed better model performances than the land cover-specific models (trained and applied only to one specific land cover). The global models performed with an R^2 of 0.85 to 0.95 and an RMSE of 0.01 to 0.03 depending on VOD wavelength (Figure 2). We also compared the model performance of a specific land cover type within the global model with the related land cover-specific model. Regarding RF models, the land cover-specific models had an R^2 of 0.09 to 0.59

295 lower and RMSE of 0.006-0.03 higher than the related land cover within the global models. Considering GAMs, land cover-specific models performed better within a certain land cover type than the global model for the same land cover type. This applies especially for land cover types with simpler vegetation structure, e.g. shrubland, herbaceous vegetation or broad-leaved evergreen trees, and less for more complex land cover types like the treeAll and short vegetation classes.

3.1.4 Effect of VOD wavelength

300 In general, the R^2 of predicting short-wavelength VOD was higher than for L-VOD predictions and RMSE decreased from long to short wavelengths (Figure 2). All SMOS L-VOD models performed with a lower R^2 and a higher RMSE than the other VOD models including SMAP L-VOD. For RF models based on 8-daily data, R^2 was highest for Ku-VOD, followed by X-VOD and C-VOD (Figure S1). For monthly data and GAMs, the order in performance was slightly different between Ku-, X- and C-VOD for R^2 and RMSE.

305 In the global model, the land cover-specific model performance depends on the different VOD wavelengths. The prediction of monthly Ku-, X- and C-VOD using RF reached the highest performance for broad-leaved evergreen trees ($0.95 \leq R^2 \leq 0.97$, $0.009 \leq$ RMSE ≤ 0.013) and the lowest performance for croplands ($0.82 \leq R^2 \leq 0.85$, $0.015 \leq$ RMSE ≤ 0.023). Predicting monthly SMAP L-VOD using RF had the highest performance in herbaceous vegetation ($R^2 = 0.93$, RMSE = 0.016) and the lowest performance in deciduous trees ($R^2 = 0.74$, RMSE = 0.031). RF prediction of monthly SMOS L-VOD attained the

310 highest performance in herbaceous vegetation ($R^2 = 0.84$, RMSE = 0.023) and the lowest performance in needle-leaved and deciduous trees and croplands ($R^2 \sim 0.6$, $0.032 \leq$ RMSE ≤ 0.059).

3.1.5 Spatial variability in model performance

Several geographical patterns of high predictability (high R^2, blue areas in Figure 3), like the cropland area in south-western and south-eastern Australia, and poor predictability (low R^2, red areas in Figure 3), e.g. southern California, are similar for all

315 VOD datasets.

Across all VOD datasets, the prediction of VOD was best in Australia; followed by South Africa, Europe, and California (Figure S3). As for the global model results (chapter 3.1.4), the best performance was achieved in predicting Ku-, X-, and C-VOD and the lowest performance for SMOS L-VOD. This is indicated by the dominant colour distribution in Figure 3 and by

the corresponding histograms (Figure S3), whereby the more right-skewed and narrower the distribution the better the
320   prediction of all pixel time series (e.g. Ku-VOD for Australia).

Not only areas with a high crop fraction have high R^2, but also areas with large shrub fractions, e.g. northern Australia and central South Africa, and high herbaceous fractions, like in north-western and south-eastern South Africa and western Australia.

Pixels with large seasonality in LAI and LFMC (e.g. eastern Europe and northern part of California), show higher R^2 results
325   per pixel. Increasing pixel land cover homogeneity also contributes to improved results. This implies worse results for more heterogeneous pixels and in regions with less pronounced seasonality in LAI due to lack of defoliation (needleleaf, evergreen), or in LFMC due to more or less stable weather conditions or to more drought resistance of less plant-water sensitivity (Rao et al., 2022), such as the central areas of California, northern Europe and central Australia. With increasing wavelength, the VOD of these areas is getting more difficult to predict.

330   Additionally, regions with mean VOD values less than 0.1 and marginal changes over time tend to have low or even negative R^2. This is noticeable in central Australia and central South Africa. The comparison of the high R^2 based on all values (section 3.1, >1.000 data samples) with the R^2 in Figure 3 and S3 shown here (monthly time series January 2015 – July 2017 resulting in a maximum time series of 31 months i.e. < 32 data samples) indicates that R^2 seems to be sensitive to the data size, leading to small R^2 when few data points are available. The reference and modelled mean VOD and the variance of VOD are highly
335   correlated in space (Spearman correlation coefficient > 0.75) which shows that the models captures the variability and spatial patterns of VOD. With higher mean VOD the R^2 increases, e.g. such as for the tree-covered areas dominated by deciduous broadleaf trees.
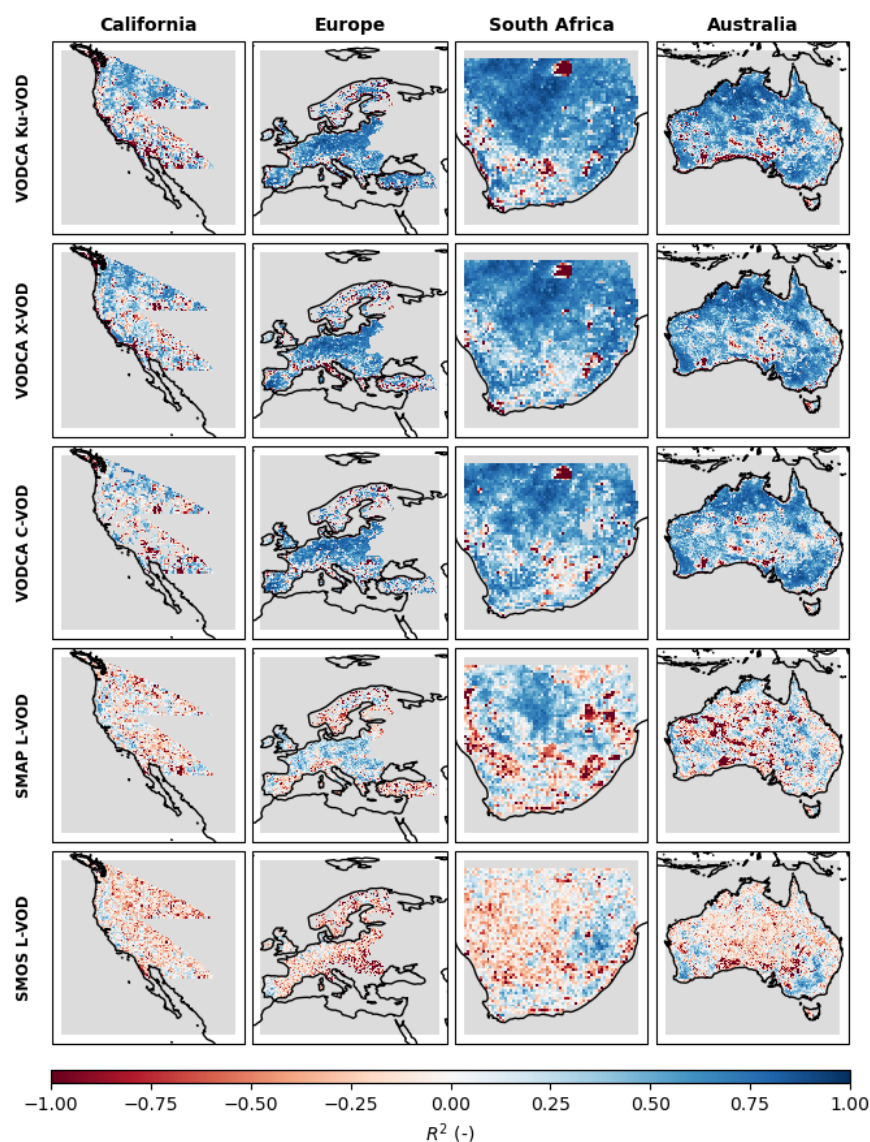
Figure 3: Coefficient of determination (R^2) per pixel for the global random forest model (PFTs included as predictor) based on monthly values. Rows indicating results for the different VOD datasets and columns the different regions as dictated by the availability of the LFMC dataset.

3.2 Relationships between VOD and vegetation properties

3.2.1 Global (inter-continental) relationships

The ALE plots in Figure 4 (Figure S4 – S7 for all global predictors based on monthly and 8-daily RF and GAM models) demonstrate the effects of vegetation properties on VOD for all wavelengths. For Ku-VOD, LAI and herbaceous land cover have the highest influence followed by AGB and LFMC with an amplitude of $\Delta_A = 0.109, 0.054, 0.045$ and 0.017, respectively. For X- and C-VOD the order of influence is LAI ($\Delta_A = 0.072$ for X-VOD; and 0.099 for C-VOD), AGB ($\Delta_A = 0.032$; and 0.046), herbaceous land cover ($\Delta_A = 0.029$; and 0.031) and LFMC ($\Delta_A = 0.017$; and 0.028).

All VOD datasets show a positive relationship with LAI, but all curves saturate around an LAI value of 2.3, which corresponds approximately to the 95%-ile of LAI in our dataset. LAI has a much stronger effect on Ku-, X-, and C-VOD than on L-VOD. Interestingly, the relationship between LAI and SMAP L-VOD (Δ_A 0.054) is more similar to the relationship of LAI and shortwave VOD e.g. X-VOD than for LAI and SMOS L-VOD (Δ_A 0.024).

355   The relationship with LFMC is more complex for all VOD datasets. From 0 % to 50 % LFMC, the relationships are negative with a negative spike at 50 % LFMC. Afterwards, VOD increases with increasing LFMC, which is most pronounced for SMOS L-VOD (overall $\Delta_A = 0.05$). However, SMAP L-VOD shows a strong negative relationship with LFMC after around 140 % LFMC (overall $\Delta_A = 0.056$).

All VOD datasets show a similar increase with AGB until 120 Mg/ha (corresponding to the 95%-ile) but the relationships
360   differ at higher AGB values. While Ku-, X- and C-VOD show a decreasing relationship with AGB, SMOS and SMAP L-VOD continue to increase (overall $\Delta_A = 0.095$ for SMOS L-VOD; and 0.107 for SMAP L-VOD).

The relationships with land cover fractions are positive for most VOD datasets. As an example, we here show the relationship with the fraction of herbaceous cover. Ku- and X-VOD show an almost monotonic increase with increasing herbaceous cover. On the other hand, C- and L-VOD (Δ_A 0.025 for SMAP; and Δ_A 0.024 for SMOS L-VOD) show a negative relationship with
365   herbaceous cover at very low coverage (up to ca. 0.15, corresponding approx. to the 40%-ile of herbaceous cover) but increase afterwards.

Taken together, we find the following effects of vegetation properties on the different VOD datasets: SMOS L-VOD is most strongly affected by AGB (positive relationship), followed by LFMC (positive relationship at LFMC > 50 %), LAI (positive relationship for LAI < 1.5), and herbaceous vegetation. SMAP L-VOD is most strongly affected by AGB (positive
370   relationship), followed by LAI (positive relationship for < 2.5), LFMC (negative relationship), and herbaceous vegetation. Ku-, X-, and C-VOD show very similar relationships and are most strongly affected by LAI (positive relationship), followed by AGB (positive relationship up to 120 Mg/ha), herbaceous vegetation cover and LFMC. The relationships with LFMC and herbaceous cover differ mostly between Ku- and X-VOD on the one hand and C-VOD on the other.

Interestingly, the amplitude of the ALE plots varies between wavelengths. For LAI and land cover a clear decrease of the ALE
375   amplitude with increasing wavelength is visible, which corresponds to the fact that the magnitude of VOD decreases with increasing wavelength. For AGB and LFMC, the ALE amplitude increases with increasing wavelength.

380
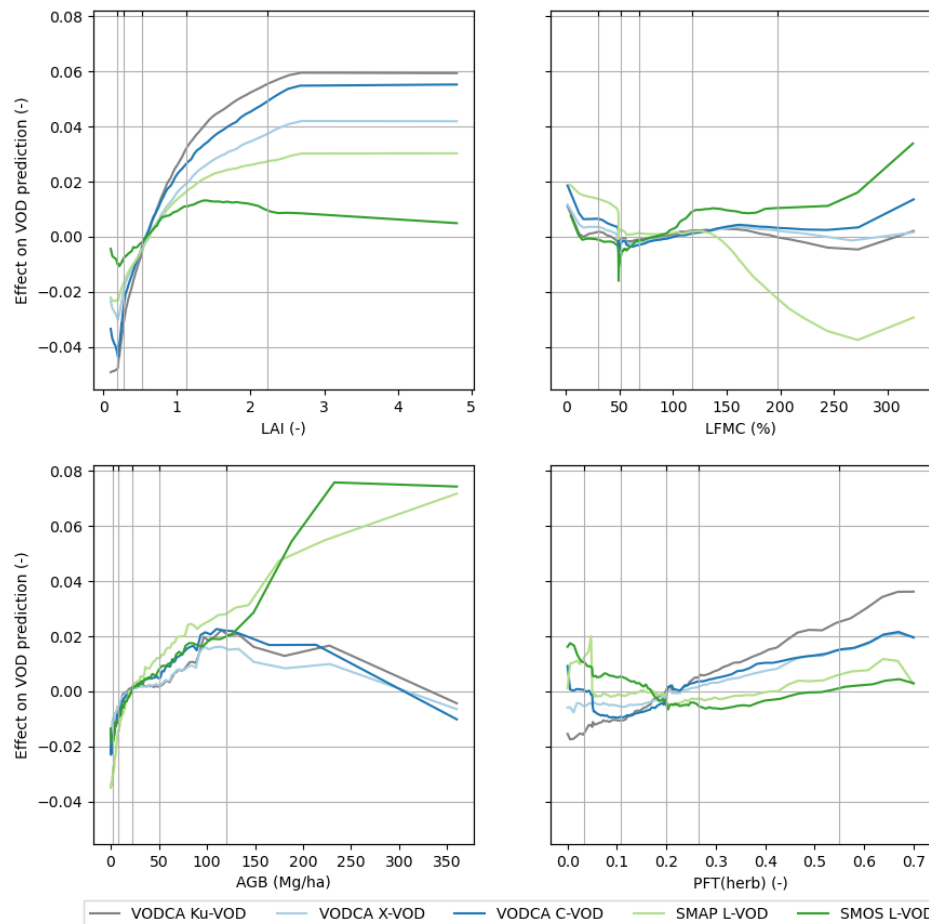
Figure 4: ALE plots of predicted normalised VOD to ecosystem properties based on the global monthly RF model with plant functional type (PFT) of herbaceous vegetation (herb) as an example of the influence of land cover fractions on VOD. Vertical lines indicate the quantiles of the data sample size 0.05, 0.25, 0.5, 0.75, and 0.95, respectively.

3.2.2 Relationships of land cover-specific models

The individual predictors in the land cover-specific models have a partially higher influence on the VOD prediction than in the global model (Figure 5, Figure S4 – S15).

For tree-covered areas (treeAll model), the LAI-ALE shows a slight positive relationship with VOD up to an LAI of ca. 2 and

385   then a stable or slightly decreasing relation. The relation with LFMC is positive for Ku-, X-, and C-VOD but unimodal for both L-VODs. AGB is the dominant predictor but the relationship with VOD is non-linear and non-monotonic.

Comparing the ALEs of the treeAll and the individual forest type models (i.e. treeB, treeN, treeD, treeE, Figure S8), the influence of a specific forest type is recognizable within the treeAll ALEs. For example, the highly non-linear relationship between VOD and LAI until LAI~2.0 is based on the VOD-LAI relationship of deciduous trees. The treeAll LFMC-ALE is

390   highly influenced by the relationship for needle-leaved and evergreen trees. The apparent SMOS L-VOD decrease with LFMC is also pronounced within most tree types but not within deciduous trees. The AGB-ALE for needle-leaved trees is less non-linear in comparison to the other tree cover models. Deciduous and broad-leaved trees exhibit a more complex relationship with AGB than evergreen and needle-leaved trees.

For short vegetation, LAI is the main influencing predictor and shows a positive relationship with all VOD bands. The ALE

395   plot between VOD and LFMC shows a similar form as in the global model with a drop around 50 % LFMC, which indicates

that the global VOD-LFMC relationship is dominated by dynamics in short vegetation areas. Particularly, the drop is based on the herbaceous land cover type, which is also visible in the 8-daily based models and in the GAMs (Figure S10, S11, S14 and S15). Contrary to the global model, the land cover–specific models do not exhibit the clear dependency of the ALE amplitude to the wavelengths. The dependency of the ALE amplitude on wavelength is still visible in the LAI-ALE of the herbaceous

400   and shrubland cover models, especially for LAI greater than 1 and more pronounced in the 8-daily based models than in the monthly based models. The same is true for the LFMC-ALE of the monthly based shrubland models above 140 % LFMC. The positive relationship between 50 % and 140 % LFMC and the following decrease (especially for the L-VOD LFMC-ALE) for short vegetation is influenced by cropland cover, because the decrease is only visible in the LFMC-ALE from the cropland model.

405
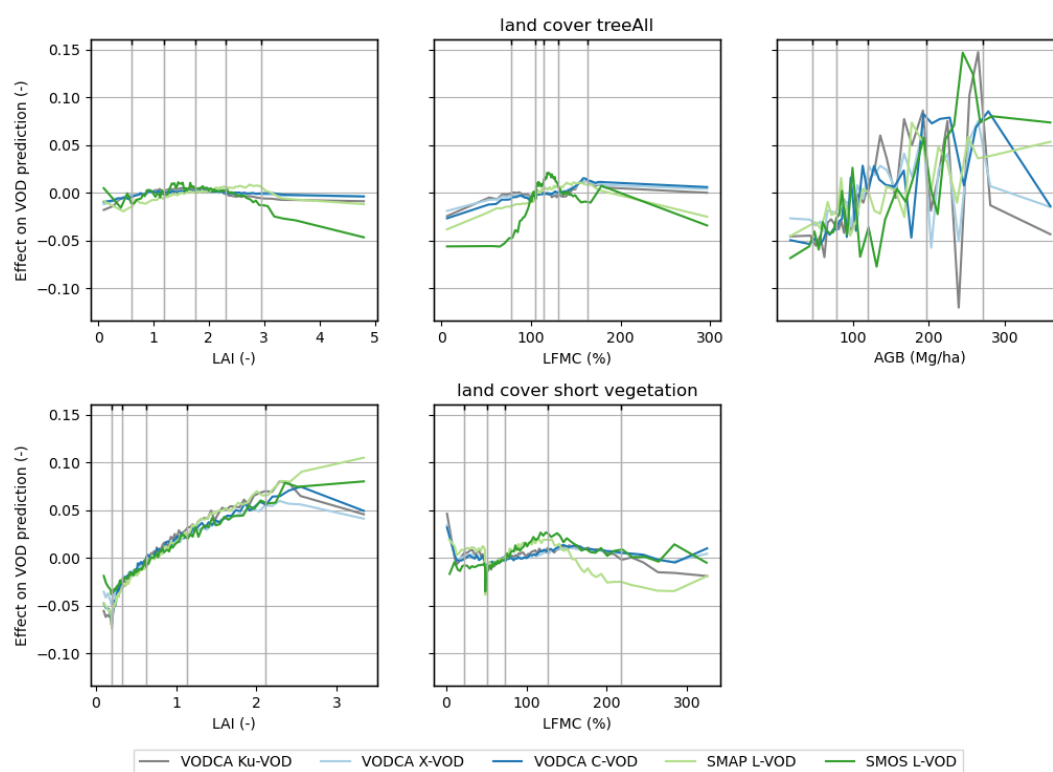
Figure 5: ALE plots of normalised VOD to ecosystem properties based on land cover-specific monthly RF models. Shown models are based on pixels with a PFT treeAll fraction more than 0.55 (top), and for short vegetation (bottom). Vertical lines indicate the quantiles of the data sample size 0.05, 0.25, 0.5, 0.75, and 0.95, respectively.

410   **4 Discussion and conclusions**

4.1 Predictors and predictability of VOD

The results demonstrate that for the global prediction of VOD, i.e. over different biomes, a more flexible modelling approach such as RF is better suited as opposed to an additive approach like GAM. The lower global performance of GAM suggests that local factors play a role in the dynamics of VOD, which were not considered and used as additional additive predictors. In

415   contrast, RF is partly able to account for this due to its ability of flexible modelling leading to better results. The simpler structure of GAM compared to RF is, in most cases, insufficient to predict VOD, but within single land cover types a simpler

additive approach like GAM is sufficient. This indicates that the relationship between VOD and ecosystem properties cannot be easily captured with global linear, monotonic, and bivariate regressions but requires accounting for the non-linear interactions between various ecosystem properties. The results imply that the set of predictors allows the estimation of the dynamics of short wavelength VODs at high temporal resolution (8-daily and monthly) with very good performance, but the set of used predictors is insufficient to explain the dynamics in L-VOD due to ignoring local effects or possibly disregarded predictors.

This conclusion is supported by the performance difference between the four studied regions. For example, Europe has a much more fragmented landscape than most areas in Australia causing mixed effects on VOD within the coarse 0.25° grid cells leading to a lower predictability in Europe than Australia. Even if PFT fractions are used as predictors, the mismatch between the coarse resolution and land cover complexity cannot be resolved. This is especially pronounced in the longwave VOD, for which the footprint is often significantly larger than 0.25° (> 40 km). A filtering of neighbouring grid cells would not then reduce the impact of the surrounding land cover. Local complex effects on VOD are related to land cover changes, intercepted, or standing water, or soil properties. For example, Saleh et al. (2006) showed for the grassland test site that because of interception L-VOD could double in value after a rainfall event. Although interception has reduced influence on the coarse resolution data (Baur et al., 2019; Wigneron et al., 2021) or might not impede temporal VOD analyses (Feldman et al., 2020), temporary flooding leads to an evident decrease in VOD. This is not only valid for short vegetation areas (Liu et al., 2019), but also for forests (Jones et al., 2011; Bousquet et al., 2021). These impacts of local effects on VOD implies that large-scale spatial relations between VOD and e.g. AGB (Liu et al., 2015; Rodríguez-Fernández et al., 2018; Mialon et al., 2020) will likely wrongly associate changes in VOD to changes in AGB, which might result in unrealistic estimates of AGB dynamics. This conclusion is supported by the findings of Konings et al. (2021), who show that regional temporal anomalies of X- and L-VOD are mostly uncorrelated with temporal anomalies of AGB but show a higher correlation with root-zone soil moisture, an indicator for water stress.

The comparison of the global and the land cover-specific models highlights the complexity of the relation between VOD and vegetation properties. An interesting result is that the ALE amplitudes (i.e. sensitivity) increase with increasing wavelength in the global model but not in the land cover-specific model. The land cover-specific models only include pixels with a coverage > 55 % of the specific land cover type but do not use PFT fractions as predictors. This indicates that PFT fractions serve as a descriptor of vegetation structure and hence as a descriptor of land cover heterogeneity in the global model. This causes a VOD-LAI relationship that varies by wavelength, but this wavelength-dependency cannot be resolved within a land cover-specific model, because it does not account for the impact of sub-pixel heterogeneity. Furthermore, the differences in the VOD-AGB relationship between the global and the land cover-specific models also highlights that a monotonic AGB-VOD relationship is only valid over a large spatial scale but does not hold within a vegetation type or at smaller scales.

The high R^2 results for high biomass areas were enabled using PFT maps as feature, which compensate for the saturating effect of AGB. Both LFMC and LAI vary in time and space and are strongly correlated. The temporal and spatial variation of our model is dominated by LAI, leading to a decreased influence of LFMC on shortwave VOD, which has a higher short-term variation than L-VOD.

Globally, the L-band VOD is highly influenced by AGB, which is in agreement with the ability of longwave VOD to better penetrate dense vegetation and its higher sensitivity to the woody plant parts (Liu et al., 2011). However, the much lower predictability of L-VOD compared to Ku-, X-, and C-VOD indicates that L-VOD cannot be sufficiently explained by the combination of AGB, LAI, LFMC, and land cover. The performance in predicting L-VOD is much lower at pixel-level (Figure 3) than computed across the spatial and temporal data. Hence, the low performance in predicting L-VOD is mostly related to the temporal dynamics because our model correctly explains the spatial patterns. The low performance in predicting SMOS L-VOD might be caused by noisy signal of the SMOS sensor (van der Schalie et al., 2017). Especially the daily raw L-VOD data, as used for the 8-daily analyses, can be very noisy (Wigneron et al., 2021). Vittucci et al. (2016) found moderate seasonal

460   differences (but within the standard variation) of the SMOS L-VOD signal over boreal forest, which are partly explainable due
to the deciduous character of the forest but moreover because of random effects. The L-band signal, and also the C-band signal,
is strongly disturbed by radio-frequency interference (RFI, Liu et al., 2019). The spatial and temporal inconsistency of RFI
complicates the RFI correction of the L-band (Wigneron et al., 2021). This indicates a noisy, or until now not fully understood,
variation of the SMOS L-VOD, especially within the lower value range. Due to the uncertain proportion of noise and short-

465   term changes of water content, Ebrahimi et al. (2018) averaged SMOS L-VOD over 15 days and Rodríguez-Fernández et
al.(2018) even over 2 years to reduce related uncertainties of the VOD signal. Vaglio Laurin et al. (2020) found a time lag of
up to 6 months for mostly tree-covered areas in South America and Africa between SMOS L-VOD and ecosystem functional
properties. This time lag shows that the relations between SMOS L-VOD and vegetation properties need further investigation
in densely-vegetated regions.

470   An interesting finding is the higher sensitivity of L-VOD to LFMC than to LAI. This indicates that L-band indeed penetrates
deeper in the canopy (low sensitivity to LAI) but is sensitive to the plant water status (i.e. LFMC). However, AGB and LFMC
are insufficient predictors to reach high predictability of L-VOD. This might be caused by the fact that the AGB dataset used
in this study does not contain any temporal information, and hence changes in AGB are not considered in our model. Using an
alternative dataset (e.g. Xu et al., 2021), which provides a global time series of AGB could be a benefit for improving the

475   understanding of temporal VOD variations. However, as we included annual land cover maps as predictors, our models do
indeed account for land cover change such as deforestation which is strongly related to a change in AGB (Andela et al., 2013).
The use of LFMC as a predictor might be insufficient for L-VOD. The LFMC data used in our study was derived from optical
observation by MODIS, which in, the case of closed forest canopies, is only sensitive to the top of the canopy. Root-zone soil
moisture was used as a proxy for water availability in other studies (e.g. Konings et al., 2021), however, it is not an ideal

480   predictor, as some plants can regulate their water potential or moisture content independent of soil moisture (Konings and
Gentine, 2017; Hochberg et al., 2018). Therefore, it is necessary to further investigate the daily to seasonal temporal dynamics
of L-VOD with respect to e.g. local and regional observations of water availability and plant water status.

4.2 Towards developing advanced approaches to link VOD with vegetation properties

The long time series, global coverage and multiple frequencies of VOD retrievals provide valuable information or can be used

485   to derive vegetation properties at large scale or to evaluate and parametrize land surface models in data assimilation studies.
Those applications of VOD require, however, a solid understanding of the biophysical controls on VOD. The relatively high
effect of LAI on the short wavelength VODs indicates that data assimilation approaches that only use LAI for estimating the
temporal dynamic of VOD (as they were used by Scholze et al., 2019 and Kumar et al., 2020) are valid approximations. This
means that even models without an explicit representation of plant water status are suitable for VOD assimilation, but the

490   observation operators need to take into account non-linear, non-additive, and local effects.
LFMC or similar measures for plant water status have only recently been introduced into land surface models commonly used
for global-scale simulations (e.g. Kennedy et al., 2019; Niu et al., 2020; Eller et al., 2020; Li et al., 2021a). LFMC has therefore
not been used in assimilation studies so far. The long time series of especially Ku-VOD could help to constrain model
simulations of LFMC or plant water studies but require a good representation of LAI dynamics.

495   For observation operators for L-VOD, AGB should be the main predictor for spatial patterns. For example, Rodríguez-
Fernández et al. (2018) modelled C-VOD from AMSR-E as an empirical function of AGB. Scholze et al. (2019) used the
empirical function between VOD and AGB evaluated by Rodríguez-Fernández et al. (2018), to simulate L-VOD from AGB.
Thereby, AGB was replaced with a function of net primary production and effective turnover time. However, temporal changes
in L-VOD might result in an overestimation in dynamics of biomass production, turnover or biomass loss if effects of changes

500   in plant water status are not considered (Konings et al., 2021). Scholze et al. (2019) tried to avoid incorporating short-term
changes due to VWC and therefore averaged the VOD simulations to yearly means. The temporal dynamics should include

the effect of plant water status, but further investigations on the drivers of the temporal dynamics of L-VOD are necessary to make full use of the data.

Including a proxy for VWC and exploring the influence of short-term changes of vegetation properties on VOD, we assessed
505   the temporal dynamics not only for L-VOD but also for Ku-, X-, and C-VOD, which will help to make explicit use of VOD temporal changes within modelling and assimilation studies.

Author contribution

LS and MF developed the research idea, objectives and methodology. LS, RvdS and MY prepared datasets. LS implemented and applied the analysis. AKR contributed to the implementation of ALE plots and the interpretation of related results. RMZ
510 and SS helped with interpreting results and reviewed the application of VOD data. LS and MF wrote the initial draft of the manuscript. All authors reviewed and revised the initial draft of the manuscript.

Competing interests

MF is guest editor of the special issue "Microwave remote sensing for improved understanding of vegetation–water interactions". The peer-review process was guided by an independent editor, and the authors have also no other competing
515 interests to declare.

Disclaimer

Special issue statement

Acknowledgements

The computations were performed on an HPC system at the Center for Information Services and High-Performance Computing
520 (ZIH) at TU Dresden. The authors thank Christopher Marrs for his detailed proofreading of this manuscript.

References

Andela, N., Liu, Y. Y., M. Van Dijk, A. I. J., De Jeu, R. A. M., and McVicar, T. R.: Global changes in dryland vegetation dynamics (1988-2008) assessed by satellite remote sensing: Comparing a new passive microwave vegetation density record
525 with reflective greenness data, 10, 6657–6676, https://doi.org/10.5194/bg-10-6657-2013, 2013.

Apley, D. W. and Zhu, J.: Visualizing the effects of predictor variables in black box supervised learning models, J. R. Stat. Soc. Ser. B Stat. Methodol., 82, 1059–1086, https://doi.org/10.1111/RSSB.12377, 2020.

530 Baur, M. J., Jagdhuber, T., Feldman, A. F., Akbar, R., and Entekhabi, D.: Estimation of relative canopy absorption and scattering at L-, C- and X-bands, Remote Sens. Environ., 233, 111384, https://doi.org/10.1016/j.rse.2019.111384, 2019.

Al Bitar, A., Mialon, A., Kerr, Y. H., Cabot, F., Richaume, P., Jacquette, E., Quesney, A., Mahmoodi, A., Tarot, S., Parrens, M., Al-Yaari, A., Pellarin, T., Rodriguez-Fernandez, N., and Wigneron, J. P.: The global SMOS Level 3 daily soil moisture
535 and brightness temperature maps, Earth Syst. Sci. Data, 9, 293–315, https://doi.org/10.5194/essd-9-293-2017, 2017.

Bousquet, E., Mialon, A., Rodriguez-Fernandez, N., Prigent, C., Wagner, F. H., and Kerr, Y. H.: Influence of surface water variations on VOD and biomass estimates from passive microwave sensors, Remote Sens. Environ., 257, 112345, https://doi.org/10.1016/j.rse.2021.112345, 2021.

540

Breiman, L.: Random Forests, Mach. Learn., 45, 5–32, https://doi.org/https://doi.org/10.1023/A:1010933404324, 2001.
Chaparro, D., Piles, M., Vall-llossera, M., Camps, A., Konings, A. G., and Entekhabi, D.: L-band vegetation optical depth

seasonal metrics for crop yield assessment, Remote Sens. Environ., 212, 249–259, https://doi.org/10.1016/j.rse.2018.04.049, 2018.

545

Dorigo, W., Moesinger, L., van der Schalie, R., Zotta, R.-M., Scanlon, T., and Jeu, R. A. M.: Long-term monitoring of vegetation state through passive microwave satellites, Bull. Am. Meteorol. Soc., 102, 110–112, 2021.

Du, J., Kimball, J. S., Jones, L. A., Kim, Y., Glassy, J., and Watts, J. D.: A global satellite environmental data record derived
550   from AMSR-E and AMSR2 microwave Earth observations, Earth Syst. Sci. Data, 9, 791–808, https://doi.org/10.5194/essd-9-791-2017, 2017.

Ebrahimi, M., Alavipanah, S. K., Hamzeh, S., Amiraslani, F., Neysani Samany, N., and Wigneron, J. P.: Exploiting the synergy between SMAP and SMOS to improve brightness temperature simulations and soil moisture retrievals in arid regions, J.
555   Hydrol., 557, 740–752, https://doi.org/10.1016/j.jhydrol.2017.12.051, 2018.

Eller, C. B., Rowland, L., Mencuccini, M., Rosas, T., Williams, K., Harper, A., Medlyn, B. E., Wagner, Y., Klein, T., Teodoro, G. S., Oliveira, R. S., Matos, I. S., Rosado, B. H. P., Fuchs, K., Wohlfahrt, G., Montagnani, L., Meir, P., Sitch, S., and Cox, P. M.: Stomatal optimization based on xylem hydraulics (SOX) improves land surface model simulation of vegetation responses
560   to climate, New Phytol., 226, 1622–1637, https://doi.org/10.1111/NPH.16419, 2020.

ESA: Land Cover CCI Product User Guide Version 2. Tech. Rep., 2017.

Fan, L., Wigneron, J. P., Xiao, Q., Al-Yaari, A., Wen, J., Martin-StPaul, N., Dupuy, J. L., Pimont, F., Al Bitar, A., Fernandez-
565   Moran, R., and Kerr, Y. H.: Evaluation of microwave remote sensing for monitoring live fuel moisture content in the Mediterranean region, Remote Sens. Environ., 205, 210–223, https://doi.org/10.1016/J.RSE.2017.11.020, 2018.

Feldman, A. F., Short Gianotti, D. J., Trigo, I. F., Salvucci, G. D., and Entekhabi, D.: Land-Atmosphere Drivers of Landscape-Scale Plant Water Content Loss, Geophys. Res. Lett., 47, https://doi.org/10.1029/2020GL090331, 2020.

570

Fernandez-Moran, R., Al-Yaari, A., Mialon, A., Mahmoodi, A., Al Bitar, A., De Lannoy, G., Rodriguez-Fernandez, N., Lopez-Baeza, E., Kerr, Y., and Wigneron, J. P.: SMOS-IC: An alternative SMOS soil moisture and vegetation optical depth product, Remote Sens., 9, 1–21, https://doi.org/10.3390/rs9050457, 2017.

575   Frappart, F., Wigneron, J. P., Li, X., Liu, X., Al-Yaari, A., Fan, L., Wang, M., Moisy, C., Le Masson, E., Lafkih, Z. A., Vallé, C., Ygorra, B., and Baghdadi, N.: Global Monitoring of the Vegetation Dynamics from the Vegetation Optical Depth (VOD): A Review, Remote Sens. 2020, Vol. 12, Page 2915, 12, 2915, https://doi.org/10.3390/RS12182915, 2020.

Friedman, J. H.: Greedy function approximation: A gradient boosting machine., 29, 1189–1232,
580   https://doi.org/10.1214/AOS/1013203451, 2001.

Hastie, T. and Tibshirani, R.: Generalized additive models: Some applications, J. Am. Stat. Assoc., 82, 371–386, https://doi.org/10.1080/01621459.1987.10478440, 1987.

585   Hastie, T., Tibshirani, R., and Friedman, J.: The Elements of Statistical Learning, https://doi.org/10.1007/978-0-387-84858-7,

2009.

Hochberg, U., Rockwell, F. E., Holbrook, N. M., and Cochard, H.: Iso/Anisohydry: A Plant–Environment Interaction Rather Than a Simple Hydraulic Trait, Trends Plant Sci., 23, 112–120, https://doi.org/10.1016/j.tplants.2017.11.002, 2018.

590

Hutengs, C. and Vohland, M.: Downscaling land surface temperatures at regional scales with random forest regression, Remote Sens. Environ., 178, 127–141, https://doi.org/10.1016/j.rse.2016.03.006, 2016.

Jackson, T. J. and Schmugge, T. J.: Vegetation effects on the microwave emission of soils, Remote Sens. Environ., 36, 203–

595 212, https://doi.org/10.1016/0034-4257(91)90057-D, 1991.

Jackson, T. J., Schmugge, T. J., and Wang, J. R.: Passive microwave sensing of soil moisture under vegetation canopies, Water Resour. Res., 18, 1137–1142, https://doi.org/10.1029/WR018I004P01137, 1982.

600 Jones, M. O., Jones, L. A., Kimball, J. S., and McDonald, K. C.: Satellite passive microwave remote sensing for monitoring global land surface phenology, Remote Sens. Environ., 115, 1102–1114, https://doi.org/10.1016/j.rse.2010.12.015, 2011.

Jones, M. O., Kimball, J. S., Small, E. E., and Larson, K. M.: Comparing land surface phenology derived from satellite and GPS network microwave remote sensing, Int. J. Biometeorol., 58, 1305–1315, https://doi.org/10.1007/s00484-013-0726-z,

605 2014.

Kennedy, D., Swenson, S., Oleson, K. W., Lawrence, D. M., Fisher, R., Lola da Costa, A. C., and Gentine, P.: Implementing Plant Hydraulics in the Community Land Model, Version 5, J. Adv. Model. Earth Syst., 11, 485–513, https://doi.org/10.1029/2018MS001500, 2019.

610

Konings, A. G. and Gentine, P.: Global variations in ecosystem-scale isohydricity, Glob. Chang. Biol., 23, 891–905, https://doi.org/10.1111/GCB.13389, 2017.

Konings, A. G., Piles, M., Das, N., and Entekhabi, D.: L-band vegetation optical depth and effective scattering albedo

615 estimation from SMAP, Remote Sens. Environ., 198, 460–470, https://doi.org/10.1016/j.rse.2017.06.037, 2017.

Konings, A. G., Rao, K., and Steele-Dunne, S. C.: Macro to micro: microwave remote sensing of plant water content for physiology and ecology, New Phytol., 223, 1166–1172, https://doi.org/10.1111/nph.15808, 2019.

620 Konings, A. G., Holtzman, N., Rao, K., Xu, L., and Saatchi, S. S.: Interannual Variations of Vegetation Optical Depth Are Due to Both Water Stress and Biomass Changes, Geophys. Res. Lett., 48, 1–9, https://doi.org/10.1029/2021gl095267, 2021.

Kuhn-Régnier, A., Voulgarakis, A., Nowack, P., Forkel, M., Prentice, I. C., and Harrison, S. P.: The importance of antecedent vegetation and drought conditions as global drivers of burnt area, 18, 3861–3879, https://doi.org/10.5194/bg-18-3861-2021,

625 2021.

Kumar, S. V., Holmes, T. R., Bindlish, R., De Jeu, R., and Peters-Lidard, C.: Assimilation of vegetation optical depth retrievals from passive microwave radiometry, Hydrol. Earth Syst. Sci., 24, 3431–3450, https://doi.org/10.5194/HESS-24-3431-2020,

2020.

630

Li, L., Yang, Z. L., Matheny, A. M., Zheng, H., Swenson, S. C., Lawrence, D. M., Barlage, M., Yan, B., McDowell, N. G., and Leung, L. R.: Representation of Plant Hydraulics in the Noah-MP Land Surface Model: Model Development and Multiscale Evaluation, J. Adv. Model. Earth Syst., 13, e2020MS002214, https://doi.org/10.1029/2020MS002214, 2021a.

635 Li, X., Wigneron, J.-P., Frappart, F., Fan, L., Ciais, P., Fensholt, R., Entekhabi, D., Brandt, M., Konings, A. G., Liu, X., Wang, M., Al-Yaari, A., and Moisy, C.: Global-scale assessment and inter-comparison of recently developed/reprocessed microwave satellite vegetation optical depth products, Remote Sens. Environ., 253, 112208, https://doi.org/10.1016/j.rse.2020.112208, 2021b.

640 Liang, L., Di, L., Huang, T., Wang, J., Lin, L., Wang, L., and Yang, M.: Estimation of leaf nitrogen content in wheat using new hyperspectral indices and a random forest regression algorithm, Remote Sens., 10, https://doi.org/10.3390/rs10121940, 2018.

Liu, R., Wen, J., Wang, X., Wang, Z., Li, Z., Xie, Y., Zhu, L., and Li, D.: Derivation of Vegetation Optical Depth and Water
645 Content in the Source Region of the Yellow River using the FY-3B Microwave Data, Remote Sens., 11, 1536, https://doi.org/10.3390/rs11131536, 2019.

Liu, Y., Holtzman, N. M., and Konings, A. G.: Global ecosystem-scale plant hydraulic traits retrieved using model-data fusion, Hydrol. Earth Syst. Sci., 25, 2399–2417, https://doi.org/10.5194/HESS-25-2399-2021, 2021.

650

Liu, Y. Y., De Jeu, R. A. M., McCabe, M. F., Evans, J. P., and Van Dijk, A. I. J. M.: Global long-term passive microwave satellite-based retrievals of vegetation optical depth, Geophys. Res. Lett., 38, 1–6, https://doi.org/10.1029/2011GL048684, 2011.

655 Liu, Y. Y., Van Dijk, A. I. J. M., De Jeu, R. A. M., Canadell, J. G., McCabe, M. F., Evans, J. P., and Wang, G.: Recent reversal in loss of global terrestrial biomass, Nat. Clim. Chang., 5, 470–474, https://doi.org/10.1038/nclimate2581, 2015.

Mialon, A., Rodríguez-Fernández, N. J., Santoro, M., Saatchi, S., Mermoz, S., Bousquet, E., and Kerr, Y. H.: Evaluation of the sensitivity of SMOS L-VOD to forest above-ground biomass at global scale, Remote Sens., 12, 1–10,
660 https://doi.org/10.3390/RS12091450, 2020.

Moesinger, L., Dorigo, W., De Jeu, R., Van Der Schalie, R., Scanlon, T., Teubner, I., and Forkel, M.: The global long-term microwave Vegetation Optical Depth Climate Archive (VODCA), Earth Syst. Sci. Data, 12, 177–196, https://doi.org/10.5194/ESSD-12-177-2020, 2020.

665

Moesinger, L., Zotta, R.-M., Schalie, R. van der, Scanlon, T., Jeu, R. de, and Dorigo, W. A.: Monitoring Vegetation Condition using Microwave Remote Sensing: The Standardized Vegetation Optical Depth Index SVODI, [preprint], in review, https://doi.org/https://doi.org/10.5194/bg-2021-360, 2022.

670 Momen, M., Wood, J. D., Novick, K. A., Pangle, R., Pockman, W. T., McDowell, N. G., and Konings, A. G.: Interacting Effects of Leaf Water Potential and Biomass on Vegetation Optical Depth, J. Geophys. Res. Biogeosciences, 122, 3031–3046,

https://doi.org/10.1002/2017JG004145, 2017.

Myneni, R., Knyazikhin, Y., Park, T.: MOD15A2H MODIS Leaf Area Index/FPAR 8-Day L4 Global 500m SIN Grid V006,
675 NASA EOSDIS L. Process. DAAC, https://doi.org/http://doi.org/10.5067/MODIS/MOD15A2H.006, 2015.

Nelder, J. A., & Wedderburn, R. W. M.: Generalized Linear Models Why Generalized Linear Models ?, J. R. Stat. Soc., 135,
370–384, https://doi.org/10.2307/2344614, 1972.

680 Niu, G. Y., Fang, Y. H., Chang, L. L., Jin, J., Yuan, H., and Zeng, X.: Enhancing the Noah-MP Ecosystem Response to
Droughts With an Explicit Representation of Plant Water Storage Supplied by Dynamic Root Water Uptake, J. Adv. Model.
Earth Syst., 12, e2020MS002062, https://doi.org/10.1029/2020MS002062, 2020.

Njoku, E. G. and Entekhabi, D.: Passive microwave remote sensing of soil moisture, J. Hydrol., 184, 101–129,
685 https://doi.org/10.1016/0022-1694(95)02970-2, 1996.

Owe, M., de Jeu, R., and Holmes, T.: Multisensor historical climatology of satellite-derived global land surface moisture, J.
Geophys. Res. Earth Surf., 113, 1–17, https://doi.org/10.1029/2007JF000769, 2008.

690 Poulter, B., MacBean, N., Hartley, A., Khlystova, I., Arino, O., Betts, R., Bontemps, S., Boettcher, M., Brockmann, C.,
Defourny, P., Hagemann, S., Herold, M., Kirches, G., Lamarche, C., Lederer, D., Ottlé, C., Peters, M., and Peylin, P.: Plant
functional type classification for earth system models: Results from the European Space Agency's Land Cover Climate Change
Initiative, Geosci. Model Dev., 8, 2315–2328, https://doi.org/10.5194/gmd-8-2315-2015, 2015.

695 Rao, K., Williams, A. P., Diffenbaugh, N. S., Yebra, M., and Konings, A. G.: Plant-water sensitivity regulates wildfire
vulnerability, Nat. Ecol. Evol. 2022 63, 6, 332–339, https://doi.org/10.1038/s41559-021-01654-2, 2022.

Rodríguez-Fernández, N. J., Mialon, A., Mermoz, S., Bouvet, A., Richaume, P., Al Bitar, A., Al-Yaari, A., Brandt, M.,
Kaminski, T., Le Toan, T., Kerr, Y. H., and Wigneron, J. P.: An evaluation of SMOS L-band vegetation optical depth (L-
700 VOD) data sets: High sensitivity of L-VOD to above-ground biomass in Africa, 15, 4627–4645, https://doi.org/10.5194/bg-
15-4627-2018, 2018.

Saleh, K., Wigneron, J. P., De Rosnay, P., Calvet, J. C., Escorihuela, M. J., Kerr, Y., and Waldteufel, P.: Impact of rain
interception by vegetation and mulch on the L-band emission of natural grass, Remote Sens. Environ., 101, 127–139,
705 https://doi.org/10.1016/j.rse.2005.12.004, 2006.

Santoro, M. and Cartus, O.: ESA Biomass Climate Change Initiative (Biomass_cci): Global datasets of forest above-ground
biomass for the year 2017, Cent. Environ. Data Anal., v1, https://doi.org/10.5285/bedc59f37c9545c981a839eb552e4084,
2019.
710
Sawada, Y., Tsutsui, H., Koike, T., Rasmy, M., Seto, R., and Fujii, H.: A field verification of an algorithm for retrieving
vegetation water content from passive microwave observations, IEEE Trans. Geosci. Remote Sens., 54, 2082–2095,
https://doi.org/10.1109/TGRS.2015.2495365, 2016.

715   van der Schalie, R., Kerr, Y. H. H., Wigneron, J. P. P., Rodríguez-Fernández, N. J. J., Al-yaari, A., Wigneron, J. P. P.,
      Rodríguez-Fernández, N. J. J., Kerr, Y. H. H., Jeu, R. A. M. d., and Schalie, R. va. V. D. Van Der: International Journal of
      Applied Earth Observation and Geoinformation Global SMOS Soil Moisture Retrievals from The Land Parameter Retrieval
      Model, Int. J. Appl. Earth Obs. Geoinf., 45, 125–134, 2016.

720   van der Schalie, R., de Jeu, R. A. M., Kerr, Y. H., Wigneron, J. P., Rodríguez-Fernández, N. J., Al-Yaari, A., Parinussa, R.
      M., Mecklenburg, S., and Drusch, M.: The merging of radiative transfer based surface soil moisture data from SMOS and
      AMSR-E, Remote Sens. Environ., 189, 180–193, https://doi.org/10.1016/j.rse.2016.11.026, 2017.

      Scholze, M., Kaminski, T., Knorr, W., Voßbeck, M., Wu, M., Ferrazzoli, P., Kerr, Y., Mialon, A., Richaume, P., Rodríguez-
725   Fernández, N., Vittucci, C., Wigneron, J. P., Mecklenburg, S., and Drusch, M.: Mean European Carbon Sink Over 2010–2015
      Estimated by Simultaneous Assimilation of Atmospheric CO2, Soil Moisture, and Vegetation Optical Depth, Geophys. Res.
      Lett., 46, 13796–13803, https://doi.org/10.1029/2019GL085725, 2019.

      Teubner, I. E., Forkel, M., Jung, M., Liu, Y. Y., Miralles, D. G., Parinussa, R., van der Schalie, R., Vreugdenhil, M., Schwalm,
730   C. R., Tramontana, G., Camps-Valls, G., and Dorigo, W. A.: Assessing the relationship between microwave vegetation optical
      depth and gross primary production, Int. J. Appl. Earth Obs. Geoinf., 65, 79–91, https://doi.org/10.1016/j.jag.2017.10.006,
      2018.

      Teubner, I. E., Forkel, M., Camps-Valls, G., Jung, M., Miralles, D. G., Tramontana, G., van der Schalie, R., Vreugdenhil, M.,
735   Mösinger, L., and Dorigo, W. A.: A carbon sink-driven approach to estimate gross primary production from microwave
      satellite observations, Remote Sens. Environ., 229, 100–113, https://doi.org/10.1016/j.rse.2019.04.022, 2019.

      Teubner, I. E., Forkel, M., Wild, B., Mösinger, L., and Dorigo, W.: Impact of temperature and water availability on microwave-
      derived gross primary production, 18, 3285–3308, https://doi.org/10.5194/bg-18-3285-2021, 2021.
740
      Vaglio Laurin, G., Vittucci, C., Tramontana, G., Ferrazzoli, P., Guerriero, L., and Papale, D.: Monitoring tropical forests under
      a functional perspective with satellite-based vegetation optical depth, Glob. Chang. Biol., 26, 3402–3416,
      https://doi.org/10.1111/gcb.15072, 2020.

745   Vittucci, C., Ferrazzoli, P., Kerr, Y., Richaume, P., Guerriero, L., Rahmoune, R., and Laurin, G. V.: SMOS retrieval over
      forests: Exploitation of optical depth and tests of soil moisture estimates, Remote Sens. Environ., 180, 115–127,
      https://doi.org/10.1016/j.rse.2016.03.004, 2016.

      Wang, J. R.: Effect of vegetation on soil moisture sensing observed from orbiting microwave radiometers, Remote Sens.
750   Environ., 17, 141–151, https://doi.org/10.1016/0034-4257(85)90070-7, 1985.

      Wang, M., Wigneron, J.-P., Sun, R., Fan, L., Frappart, F., Tao, S., Chai, L., Li, X., Liu, X., Ma, H., Moisy, C., and Ciais, P.:
      A consistent record of vegetation optical depth retrieved from the AMSR-E and AMSR2 X-band observations, Int. J. Appl.
      Earth Obs. Geoinf., 105, 102609, https://doi.org/10.1016/J.JAG.2021.102609, 2021.
755
      Wigneron, J. P., Calvet, J. C., Kerr, Y., Chanzy, A., and Lopes, A.: Microwave Emission of Vegetation: Sensitivity to Leaf
      Characteristics, IEEE Trans. Geosci. Remote Sens., 31, 716–726, https://doi.org/10.1109/36.225537, 1993.

Wigneron, J. P., Mialon, A., De Lannoy, G., Fernandez-Moran, R., Al-Yaari, A., Ebrahimi, M., Rodriguez-Fernandez, N.,
760 Kerr, Y., Quets, J., Pellarin, T., Fan, L., Tian, F., Fensholt, R., and Brandt, M.: SMOS-IC: Current status and overview of soil moisture and VOD applications, Int. Geosci. Remote Sens. Symp., 2018-July, 1451–1454, https://doi.org/10.1109/IGARSS.2018.8519382, 2018.

Wigneron, J. P., Li, X., Frappart, F., Fan, L., Al-Yaari, A., De Lannoy, G., Liu, X., Wang, M., Le Masson, E., and Moisy, C.:
765 SMOS-IC data record of soil moisture and L-VOD: Historical development, applications and perspectives, Remote Sens. Environ., 254, 112238, https://doi.org/10.1016/J.RSE.2020.112238, 2021.

Wild, B., Teubner, I., Moesinger, L., Zotta, R.-M., Forkel, M., van der Schalie, R., Sitch, S., and Dorigo, W.: VODCA2GPP – a new, global, long-term (1988–2020) gross primary production dataset from microwave remote sensing, Earth Syst. Sci.
770 Data, 14, 1063–1085, https://doi.org/10.5194/ESSD-14-1063-2022, 2022.

Xu, L., Saatchi, S. S., Yang, Y., Yu, Y., Pongratz, J., Anthony Bloom, A., Bowman, K., Worden, J., Liu, J., Yin, Y., Domke, G., McRoberts, R. E., Woodall, C., Nabuurs, G. J., De-Miguel, S., Keller, M., Harris, N., Maxwell, S., and Schimel, D.: Changes in global terrestrial live biomass over the 21st century, Sci. Adv., 7,
775 https://doi.org/10.1126/SCIADV.ABE9829/SUPPL_FILE/ABE9829_SM.PDF, 2021.

Yebra, M., Quan, X., Riaño, D., Rozas Larraondo, P., van Dijk, A. I. J. M., and Cary, G. J.: A fuel moisture content and flammability monitoring methodology for continental Australia based on optical remote sensing, Remote Sens. Environ., 212, 260–272, https://doi.org/10.1016/j.rse.2018.04.053, 2018.
780
Yee, T. W. and Mitchell, N. D.: Generalized additive models in plant ecology, J. Veg. Sci., 2, 587–602, https://doi.org/10.2307/3236170, 1991.

Zhang, Y., Zhou, S., Gentine, P., and Xiao, X.: Can vegetation optical depth reflect changes in leaf water potential during soil
785 moisture dry-down events?, Remote Sens. Environ., 234, 111451, https://doi.org/10.1016/J.RSE.2019.111451, 2019.